ISSN 0036-0236, Russian Journal of Inorganic Chemistry, 2015, Vol. 60, No. 7, pp. 804–816. © Pleiades Publishing, Ltd., 2015.
Original Russian Text © N.A. Zakharov, Zh.A. Ezhova, E.M. Koval', V.T. Kalinnikov, A.G. Tkachev, 2015, published in Zhurnal Neorganicheskoi Khimii, 2015, Vol. 60, No. 7, pp. 887–900.

Synthesis and Physicochemical Characteristics of the Calcium Hydroxyapatite/Graphene Oxide Hybrid Nanocomposite

N. A. Zakharov[a], Zh. A. Ezhova[a], E. M. Koval'[a], V. T. Kalinnikov[a, †], and A. G. Tkachev[b]

[a] *Kurnakov Institute of General and Inorganic Chemistry, Russian Academy of Sciences, Leninskii pr. 31, Moscow, 119991 Russia*

[b] *Tambov State Technical University, ul. Sovetskaya 106, Tambov, 392000 Russia*

e-mail: zakharov@igic.ras.ru

Received October 28, 2014

Abstract—The system $CaCl_2$–$(NH_4)_2HPO_4$–NH_3–H_2O–graphene oxide (25°C) was studied by the solubility method (Tananaev's residual concentration method) and by pH measurements and was used to model in vitro the biomineralization of the main inorganic component of the bone tissue—calcium hydroxyapatite (HA) $Ca_{10}(PO_4)_6(OH)_2$—in the presence of a nanosized modification of carbon—graphene oxide (GO). It was shown that the synthesis in the system produces hybrid composite materials (CM) of the general composition $Ca_{10}(PO_4)_6(OH)_2 \cdot xGO \cdot yH_2O$, where $x = 0.5$, 1.0, and 2.0 and $y = 7.4$–7.7, which contain GO and nanocrystalline (NC) HA of the stoichiometric composition. By chemical analysis, X-ray powder diffraction analysis, IR spectroscopy, thermogravimetric analysis, and differential scanning calorimetry, the main physicochemical characteristics of the synthesis products were determined, the effect of the composition on the crystallographic parameters, sizes, and morphology of NC HA in HA/GO CM was evaluated, and the main composition–structure–dispersity–properties relationships for the synthesized HA/GO CM were analyzed.

DOI: 10.1134/S0036023615070177

Although there has been a considerable increase in the number of studies of technical and medical applications of graphene and its analogues, including graphene oxide (GO), there is currently only insignificant information on their interaction with biological systems and their toxicity [1]. Fragmentary literature data on the in vitro toxicity of graphene materials suggest that, just as in other carbon nanomaterials, features of their physicochemical characteristics can play a significant role in the biological activity of this new class of materials [2].

Available data on the cytotoxic effect of graphene nanomaterials, disruption of the plasma membrane, disturbance of the mitochondrial activity, generation of oxidative stress, and damage to protein molecules, causing neuronal cell death, are all indicative of the toxicity of such materials [3–5]. However, such data are often preliminary, somewhat contradictory, and largely dependent on the properties of the graphene-like nanomaterials used [6, 7].

GO is an allotropic form of carbon, has two-dimensional structure, and consists of one or several layers of a hexagonal crystal lattice of carbon atoms with sp^2-hybridization [8]. GO is typically produced by sonication of graphite oxide [9].

The potential of using GO for producing medical composite materials (CM) and the increasing use of GO in the industry make topical the problem of determining features of its interaction with native tissues, in particular, with the bone tissue.

Calcium hydroxyapatite (HA) $Ca_{10}(PO_4)_6(OH)_2$ is the main inorganic component of the bone tissue [11–13]. Owing to high biocompatibility and bioactivity, HA is widely used in medicine as an implant material and in bone tissue engineering [14, 15]. Biological apatites of native tissues of mammals are the main (~60%) components of the bone and dental tissues and are nanosized (~5–50 nm) crystals with an acicular habit with cation and anion substitutions in the crystal structure of HA [15, 16]. Stoichiometric nanocrystalline (NC) HA is a crystal chemical analogue of the inorganic component of mineralized tissues of mammals and is a model object for studying the effect of various factors on the physicochemical and medical and biological characteristics of the inorganic component of the bone and dental tissues.

In this work, we investigated the interaction of GO with HA (an analogue of the inorganic component of the bone tissue) in the course of an in vitro model experiment simulating the biomineralization in the presence of insignificant amounts of GO as a contaminant. The GO interaction with biocompatible HA and the HA/GO CM synthesis were evaluated using aqueous solutions of calcium and phosphorus salts in the system $CaCl_2$–$(NH_4)_2HPO_4$–NH_3–H_2O–GO (25°C) containing GO as a contaminant. The physic-

† Deceased.

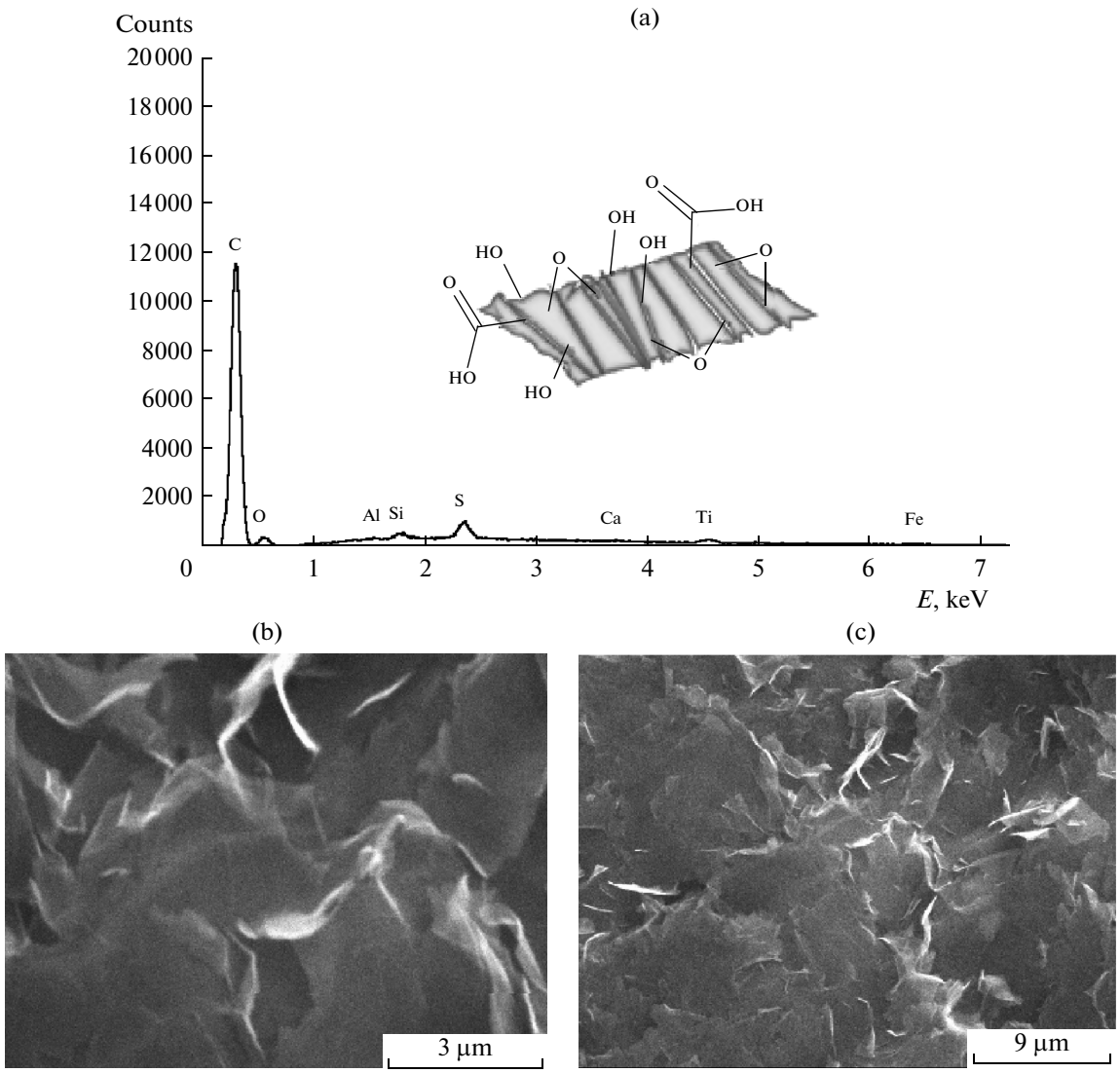

Fig. 1. (a) Electron spectroscopy for chemical analysis showed that the GO samples used for the synthesis contained ~90 wt % carbon, ~10 wt % oxygen, and traces of Al, Si, S, Ca, Ti, and Fe (b, c). Scanning electron microscopy images of the GO samples used for the synthesis at various magnifications.

ochemical characteristics of the synthesis products were determined by chemical analysis, X-ray powder diffraction analysis, IR spectroscopy, thermogravimetric analysis, and differential scanning calorimetry.

EXPERIMENTAL

Methods of Investigation

In the equilibrium liquid phase forming by the interaction of the initial precursors, pH was measured by an I160MI ion meter, the Ca^{2+} ion concentration was determined by EDTA titration, and the phosphorus (phosphorus complexes) content was found by the photometric vanadate–molybdatNe method. The nitrogen and carbon contents of the synthesized solid phases were determined by CH analysis with a Carlo Erba EA 1108 elemental analyzer.

The X-ray powder diffraction analysis and the determination of the crystallographic characteristics and crystal sizes of the synthesis products were performed with a DRON-4 automated diffractometer (CuK_α radiation, graphite monochromator, EXPRESS control program). The modified full-profile analysis and the estimation of Cauchy block sizes D_{hkl} and crystal lattice microstrains were made using the PHAN and PHAN% programs.

The IR diffuse reflectance spectra of the synthesis products were recorded within the range 4000–400 cm^{-1} with a Nicolet NEXUS FT-IR spectrometer.

The thermal characteristics of the initial GO were measured in air by thermogravimetric analysis with a

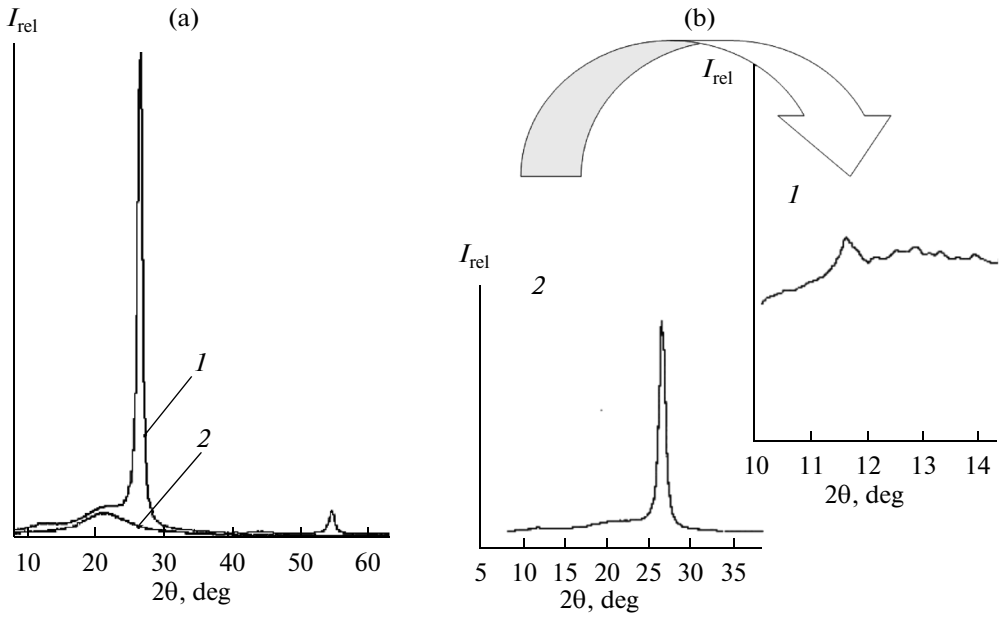

Fig. 2. (a) (*1*) X-ray powder diffraction pattern of GO and (*2*) the background of amorphous quartz (cell). (b) (*1*) The magnified image of a small-angle portion of (*2*) the X-ray powder diffraction pattern of GO.

Universal V4.4A TA Instruments analyzer and by differential scanning calorimetry with a DSC Q100 V9.8 Build instrument within the temperature range 20–700°C. The thermal characteristics of the synthesis products in a He atmosphere within the temperature range 20–1000°C were found with an STA 409 simultaneous thermal analyzer.

The structure and chemical composition of the initial GO samples were determined with a CamScanS4 scanning electron microscope equipped with a Linc Analytical microanalyzer and with a JEOL JEM 1210 electron microscope.

Physicochemical Identification of the Initial GO

GO was obtained from natural graphite powder by a modified method described previously [17, 18].

Table 1. Types and frequencies of vibrations of bonds in various functional groups of GO

Type of vibration	Vibration frequency, cm^{-1}
OH	3398
C=O COOH	1730
C=C	1623
C–OH	1348
C–O	1054
C–O–C	833

Electron spectroscopy for chemical analysis showed that the carbon and contents of the initial GO were ~90 and ~10 % wt %, respectively (Fig. 1a). In the scanning electron microscopy images, GO layers have a typical shape of rugose sheets (Figs. 1b, 1c).

The weak peak at $2\theta \approx 11°$ in the X-ray powder diffraction pattern of the initial GO (Figs. 2a, 2b) indicates insignificant interplanar spacing and crystallographic ordering of GO [18]. The X-ray powder diffraction pattern bears a certain semblance to the diffraction characteristics of graphite with a hexagonal symmetry (layer sequence *AB*, structural type *A*9*a*, Pearson symbol *hP*4). The peak at $2\theta = 13°$ suggests the presence of amorphous carbon in the initial carbon material, and the peak at $2\theta = 26°$ is characteristic of carbon in the form of graphite [19–21]. The background was reflections from the quartz cell (Fig. 2a, curve *2*).

Amorphous carbon (Figs. 3a, 3b) in the initial GO (Fig. 3c) in the transmission electron microscopy images manifests itself as individual particles ~200 nm in size, which form agglomerates ~400 nm in size (Figs. 3a, 3b).

The thermogravimetric curves of the initial GO (Fig. 4) show that the GO decomposition is a multistep process. Water molecules adsorbed on the GO surface evaporate within the temperature range 50–150°C. Decarboxylation begins within the temperature range 150–350°C. At higher temperatures of 350–500°C, hydroxyl groups bonded to GO sheets are removed. Thermal oxidation of GO carbon occurs near 550°C.

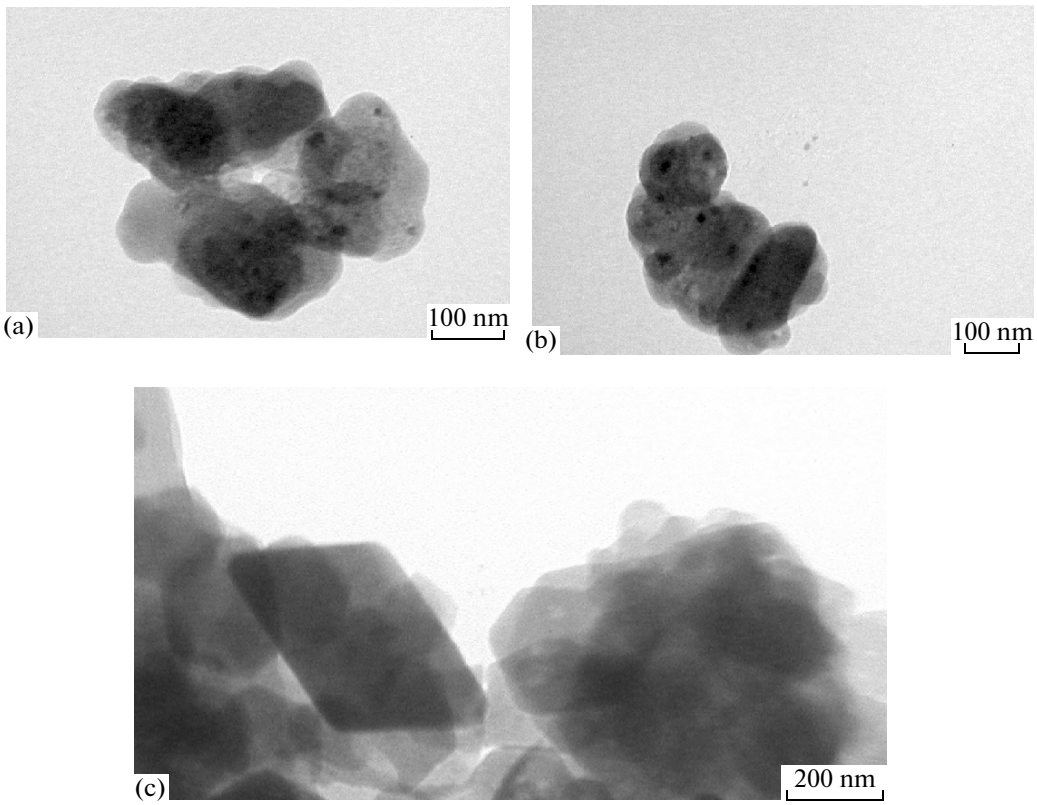

Fig. 3. Scanning electron microscopy images of (a, b) amorphous carbon particles in the initial GO and (c) GO sheets.

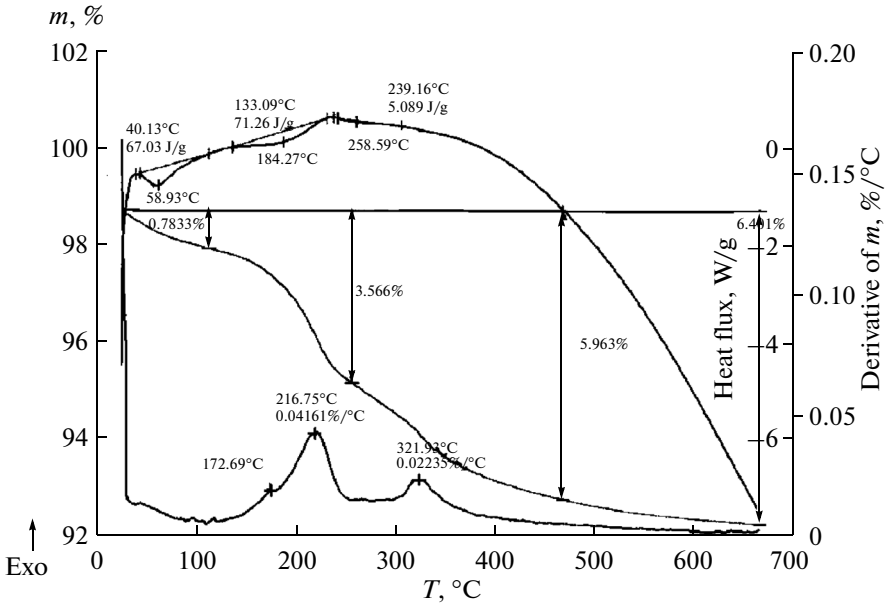

Fig. 4. Thermogravimetric and differential scanning calorimetry curves of the initial GO.

The IR spectra of the initial aqueous GO paste (Table 1, Fig. 5a) have a broad absorption band of adsorbed water with the center at 3398 cm^{-1} (stretching of hydroxyl groups –OH). The vibrations at 1730 cm^{-1} are the stretching vibrations of carboxyl groups –COOH or coupled carbonyl groups –C=O on the edges of carbon sheets. At 1623 cm^{-1}, there is a band of stretching vibrations of C=C bonds. The stretching vibrations of

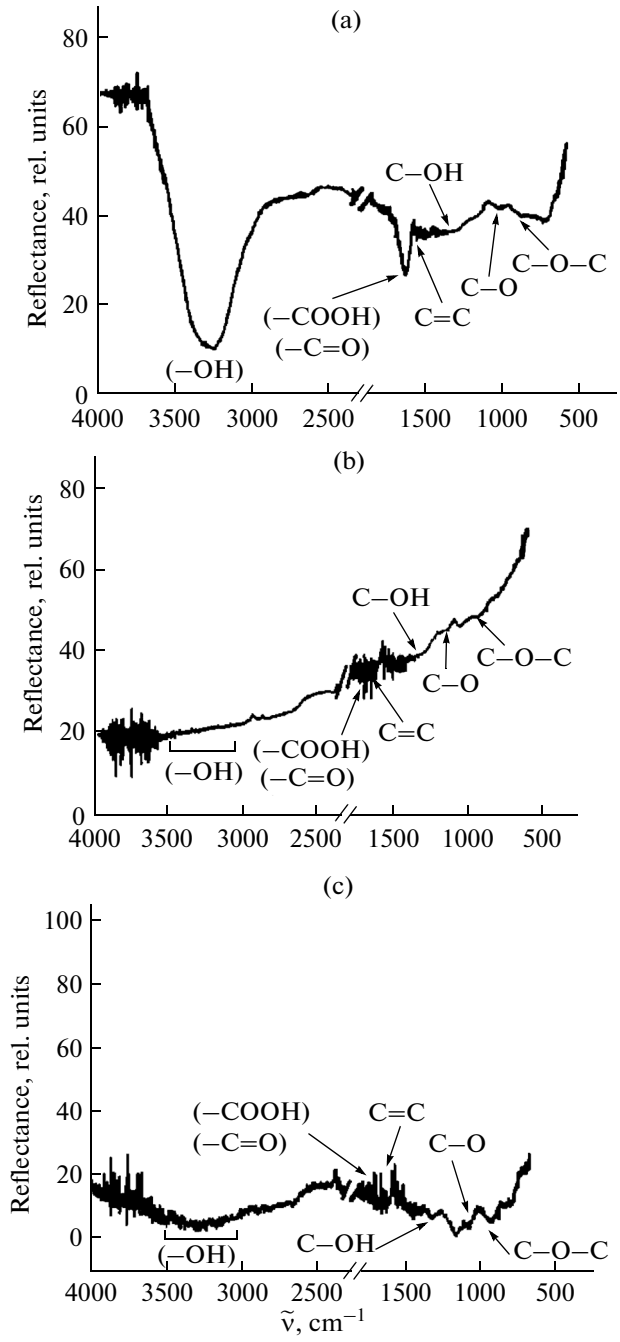

Fig. 5. IR reflectance spectra of GO: (a) initial GO (GO paste/water), (b) initial GO dried at 50°C, and (c) aqueous GO dispersion sonicated and dried at 50°C.

C–OH manifest themselves a weak band at 1226 cm^{-1}. The stretching vibrations of C–O give raise to a weak band with the center at 1054 cm^{-1}. Epoxy groups on the carbon sheet surface are characterized by the absorption band at 833 cm^{-1}.

The IR spectrum of the dried GO paste virtually lacks the absorption bands assigned to adsorbed water and vibrations of carboxyl groups –COOH and coupled carbonyl groups –C=O on the edges of carbon sheets (Fig. 5b). The stretching vibrations of C–O and the vibrations of epoxy groups remain almost unchanged. Sonication of a GO dispersion with subsequent drying leads to similar results, with the difference that a certain amount of adsorbed water remains (Fig. 5c).

Synthesis of Objects of Investigation

HA and HA/GO CM were obtained by precipitation from aqueous solutions in the systems $CaCl_2$–$(NH_4)_2HPO_4$–NH_3–H_2O (25°C) and $CaCl_2$–$(NH_4)_2HPO_4$–NH_3–H_2O–GO (25°C), respectively. The initial components were an aqueous $CaCl_2$, $(NH_4)_2HPO_4$ solutions, aqueous ammonia, and an aqueous GO dispersion. The aqueous GO dispersion for the synthesis was produced from the initial aqueous GO paste by treatment in a GRAD 13-55 sonication bath for 0.5 h at a frequency of 55 kHz and a power of 55 W.

The synthesis was carried out at constant concentrations of $(NH_4)_2HPO_4$ (0.02 mol) and ammonium hydroxide (10 ml of concentrated ammonia solution) and at a pH of the reaction mixture of 10–10.3 (to prevent the formation of tricalcium phosphate). The ratios of the initial components in the mixtures were $n_1 = CaCl_2 : (NH_4)_2HPO_4 = 1.67$ and $n_2 = GO : (NH_4)_2HPO_4 = 0.083–0.33$. In the course of the synthesis, a $CaCl_2$ solution was added to the aqueous GO dispersion and precipitation was performed by adding a mixed solution containing $(NH_4)_2HPO_4$ and ammonia. The synthesis was conducted while intensely stirring with a magnetic stirrer for 14 days in a volume of 200 ml until complete equilibrium in the system was reached according to the previously established [22] conditions for producing stoichiometric HA in the system $CaCl_2$–$(NH_4)_2HPO_4$–NH_3–H_2O (25°C).

By analyzing the equilibrium liquid phases after completion of the synthesis reaction, the Ca^{2+} and PO_4^{3-} ion contents were determined, and the molar ratios $n_3 = Ca^{2+}/PO_4^{3-}$ and $n_4 = GO/PO_4^{3-}$ in the solid phases were calculated. The solid phases used for the analysis were filtered off, washed with distilled water until pH 7, and dried in air at atmospheric temperature until constant weight.

Physicochemical Analysis and Properties of the Synthesis Products

Chemical analysis of the synthesis products. The experimental design was such that the precipitation from the solution gave either single-phase stoichiometric (Ca : P = 1.67) HA (in the system $CaCl_2$–$(NH_4)_2HPO_4$–NH_3–H_2O (25°C), $n_1 = 1.67$, pH 10.2 (Table 2) [22]), or stoichiometric HA (in the system $CaCl_2$–$(NH_4)_2HPO_4$–NH_3–H_2O–GO (25°C)) in HA/GO CM (Table 2).

Table 2. Residual concentrations and the composition of the synthesis products in the systems $CaCl_2$–$(NH_4)_2HPO_4$–NH_3–H_2O (25°C) and $CaCl_2$–$(NH_4)_2HPO_4$–NH_3–H_2O–GO (25°C)*

No. of test	n_2	pH	Found in solution, g-ion/L × 10^3		n_3	n_4	Solid phase composition
			Ca^{2+}	PO_4^{3-}			
System $CaCl_2$–$(NH_4)_2HPO_4$–NH_3–H_2O (25°C)							
1	–	10.2	0.3	0.2	1.67	–	$Ca_{10}(PO_4)_6(OH)_2 \cdot 6H_2O$
System $CaCl_2$–$(NH_4)_2HPO_4$–NH_3–H_2O–GO (25°C)							
2	0.083	10.2	0.3	0.2	1.67	0.083	$Ca_{10}(PO_4)_6(OH)_2 \cdot 0.5GO \cdot 7.6H_2O$
3	0.167	10.0	0.3	0.2	1.67	0.167	$Ca_{10}(PO_4)_6(OH)_2 \cdot GO \cdot 7.4H_2O$
4	0.33	10.1	0.3	0.2	1.67	0.33	$Ca_{10}(PO_4)_6(OH)_2 \cdot 2GO \cdot 7.7H_2O$

* In the initial mixtures, the $(NH_4)_2HPO_4$ concentration is 0.02 mol/L, $n_1 = CaCl_2 : (NH_4)_2HPO_4 = 1.67$, and $n_2 = GO : (NH_4)_2HPO_4$. Stirring time is 14 days.

In the solid phases, $n_3 = Ca^{2+}/PO_4^{3-}$; $n_4 = GO/PO_4^{3-}$.

Table 3. Results of the chemical analysis of the synthesis products in the systems $CaCl_2$–$(NH_4)_2HPO_4$–NH_3–H_2O (25°C) and $CaCl_2$–$(NH_4)_2HPO_4$–NH_3–H_2O–GO (25°C)*

Composition of synthesis products	Content, wt %					
	Ca	P	OH	H_2O	GO	weight loss (1000°C)
$Ca_{10}(PO_4)_6(OH)_2 \cdot 6H_2O$	35.91 / 36.02	16.67 / 16.72	3.05 / 3.05	9.97 / 9.71	–	9.97 / 9.71
$Ca_{10}(PO_4)_6(OH)_2 \cdot 0.5GO \cdot 7.6H_2O$	34.70 / 34.68	16.11 / 16.10	2.94 / 2.94	11.78 / 11.84	1.21 / 1.21	12.99 / 13.05
$Ca_{10}(PO_4)_6(OH)_2 \cdot GO \cdot 7.4H_2O$	34.36 / 34.37	15.94 / 15.95	2.92 / 2.92	11.47 / 11.42	2.40 / 2.40	13.87 / 13.82
$Ca_{10}(PO_4)_6(OH)_2 \cdot 2GO \cdot 7.7H_2O$	33.40 / 33.42	15.50 / 15.51	2.83 / 2.83	11.60 / 11.56	4.67 / 4.67	16.27 / 16.23

* The numerator and denominator contain the found and calculated values, respectively.

The results of the physicochemical analysis of the interaction between calcium and phosphorus salts and GO in the systems $CaCl_2$–$(NH_4)_2HPO_4$–NH_3–H_2O (25°C) and $CaCl_2$–$(NH_4)_2HPO_4$–NH_3–H_2O–GO (25°C) under biomimetic conditions (Table 2) are based on the data of the chemical analysis of the intermediate phases and the synthesis products, on the determination of the phase compositions and the crystallographic characteristics by X-ray powder diffraction analysis, and on the thermal analysis data. The obtained results showed that the composition of the synthesis products is mainly determined by the Ca : P ratio between the reacting precursors. The basis of the forming CM is stoichiometric HA. A change in the GO content hardly influences the composition of the forming calcium phosphates (HA) in the synthesized CM. The GO content of the produced CM is close to that of the initial reactive mixtures.

The determination of the solubility (residual concentrations) (Table 2) demonstrated that, regardless of the GO concentration in the initial mixtures, the equilibrium liquid phases after the completion of the synthesis reaction contain insignificant amounts of Ca^{2+} and PO_4^{3-} ions (0.0002 and 0.00012 g-ion/L, respectively). Under the chosen synthesis conditions (n_1 = 1.67, pH 10–10.3, mixture stirring time 14 days), in the interaction between $CaCl_2$ and $(NH_4)_2HPO_4$, almost all of the Ca^{2+} and PO_4^{3-} ions pass to the solid phase. The ratios $Ca^{2+} : PO_4^{3-}$ in the solid phases as cal-

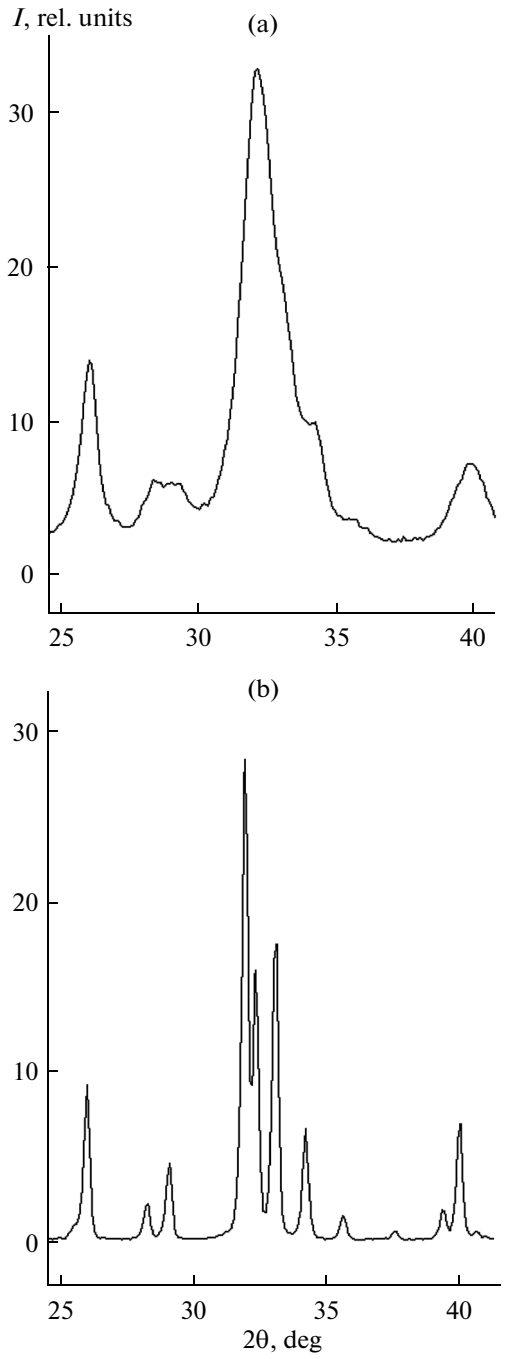

Fig. 6. Characteristic regions of the X-ray powder diffraction patterns of NC HA in HA/GO CM $Ca_{10}(PO_4)_6(OH)_2 \cdot 2GO \cdot 7.7H_2O$ (Table 2, test 4) (a) before and (b) after annealing (100°C, 1 h).

culated by the data of the analysis of the equilibrium liquid phases are 1.67, which is indicative of the formation of stoichiometric HA in HA/GO CM.

After the completion of the HA/GO CM synthesis, settling, and precipitation of the solid phase, the liquid phase was transparent. The color of the precipitates varied depending on the GO content of the forming HA/GO CM from light-gray (Table 2, test 2) to shades of black (Table 2, tests 3, 4).

The results of the chemical and NCH (Table 3) analyses suggested that all of the GO has passed to the solid synthesis products (Table 2, tests 2–4), which are homogeneous nanosized CM containing NC HA and GO with the general formula $Ca_{10}(PO_4)_6(OH)_2 \cdot xGO \cdot yH_2O$, where $x = 0.5$, 1.0, and 2.0 and $y = 7.4$–7.7.

X-ray powder diffraction analysis of the synthesis products. The results of the X-ray powder diffraction analysis of the powdered synthesis products suggested that the synthesis in the system $CaCl_2$–$(NH_4)_2HPO_4$–NH_3–H_2O (25°C) gives single-phase stoichiometric NC HA with a hexagonal symmetry (space group $P6_3/m$). The synthesis in the system $CaCl_2$–$(NH_4)_2HPO_4$–NH_3–H_2O–GO (25°C) produces homogeneous HA/GO CM containing stoichiometric NC HA and GO of the composition $Ca_{10}(PO_4)_6(OH)_2 \cdot xGO \cdot yH_2O$, where $x = 0.5$, 1.0, and 2.0 and $y = 7.4$–7.7.

The presence of GO in CM had no significant effect on the X-ray diffraction pattern of NC HA (Fig. 6a) in comparison with that of single-phase stoichiometric NC HA (Fig. 6b). NC HA particles are elongated along the *c* axis and have sizes and crystallographic characteristics similar to those for NC apatites of native bone [15]. The unit cell parameters of the synthesized HA (Table 4) are close to tabular data (JCPDS, no. 9-432 [23]).

IR spectroscopy. The IR spectra of the synthesis products (individual stoichiometric NC HA and NC HA in HA/GO CM) (Fig. 7) are typical of stoichiometric NC HA and have characteristic absorption bands related to the main structural groupings of HA. All the characteristic reflections of HA/GO CM are determined by the predominant reflections of NC HA. As in the spectrum of native apatite of the bone tissue, the band ν(OH) at 3570 cm^{-1} is weak. The bands of stretching vibrations of PO_4^{3-} groups are at 1092 (diffuse shoulder), 1033, and 963 cm^{-1}. The bending vibrations of PO_4^{3-} groups are represented by bands at 604, 566, and 470 cm^{-1}.

In the synthesis in air, there is carbonization of NC HA, which is similar to carbonization of native apatites. Carboxyl groups CO_3^{2-} are characterized by absorption bands at 1482, 1420, and 875 cm^{-1}, which is indicative of partial substitution of carboxyls for both hydroxyl groups OH^- (type A substitution) and PO_4^{3-} groups (type B substitution) (Fig. 7). The high sorption capacity owing to the developed surface of NC HA in individual HA and in HA in HA/GO CM (Table 2) gives rise to a significant background within the range 3500–2900 cm^{-1} and a band of bending vibrations of H–O–H groupings at 1671 cm^{-1}. The results of IR spectroscopy showed that NC HA in HA/GO CM has all the main features of individual NC HA (Fig. 7). All the relative intensities of the main

Table 4. Crystallographic and morphological characteristics of the synthesized NC of individual stoichiometric HA and NC HA in HA/GO CM*

Composition of composites	a, Å	c, Å	Cauchy block size, nm	
			$\parallel c$	$\perp c$
$Ca_{10}(PO_4)_6(OH)_2 \cdot 6H_2O$	9.4274 ± 0.0005	6.8808 ± 0.0002	23.3	12.3
$Ca_{10}(PO_4)_6(OH)_2 \cdot 0.5GO \cdot 7.6H_2O$	9.4258 ± 0.0003	6.8794 ± 0.0002	15.9	8.6
$Ca_{10}(PO_4)_6(OH)_2 \cdot GO \cdot 7.4H_2O$	9.4224 ± 0.0003	6.8749 ± 0.0002	15.3	8.8
$Ca_{10}(PO_4)_6(OH)_2 \cdot 2GO \cdot 7.7H_2O$	9.4282 ± 0.0005	6.8778 ± 0.0003	18.6	11.3
$Ca_{10}(PO_4)_6(OH)_2 \cdot 2GO \cdot 6.5H_2O$ (1000°C)	9.4195 ± 0.0005	6.8848 ± 0.0005	182.8	
$Ca_{10}(PO_4)_6(OH)_2$	9.418 [23]	6.884 [23]		

* $\parallel c$ and $\perp c$ are the sizes of NC HA crystallites along and across the hexagonal c axis, respectively.

structural groupings of apatites HA in HA/GO CM experienced no significant changes in comparison with individual NC HA. A certain decrease in the intensities of the lines of hydroxyl groups OH^- in NC HA in HA/GO CM at 3570 cm^{-1} was previously noted for a number of composites based on NC HA [24, 25].

Thermogravimetric analysis. On heating HA/GO CM (Table 2, test 4) to 1000°C in a He atmosphere, there was continuous weight loss (Fig. 8). The primary weight loss within the temperature range 80–100°C is due to the removal of weakly bonded adsorbed water (~0.5%) from the composite. The insignificant endothermic event within the temperature range 950–1000°C describes the removal of a small (~1%) amount of carbonate contained in HA/GO CM. The total weight loss on heating HA/GO CM to 1000°C in

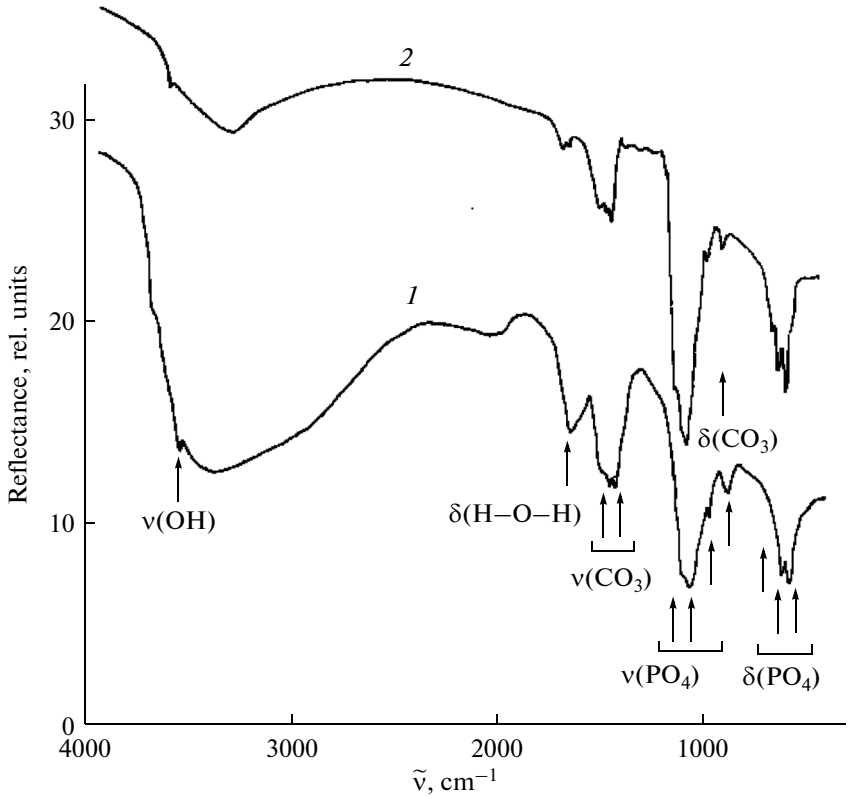

Fig. 7. IR diffuse reflectance spectra of (*1*) NC HA and (*2*) and HA/GO CM of the composition $Ca_{10}(PO_4)_6(OH)_2 \cdot xGO \cdot yH_2O$, where $x = 2.0$ and $y = 7.7$.

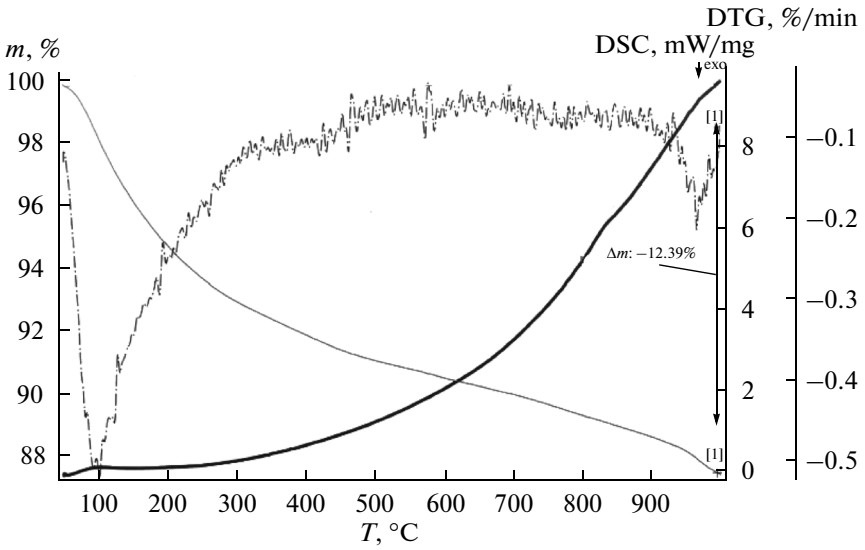

Fig. 8. Thermogravimetric and differential scanning calorimetry curves of HA/GO CM of the composition $Ca_{10}(PO_4)_6(OH)_2 \cdot xGO \cdot yH_2O$, where $x = 2.0$ and $y = 7.7$.

a He atmosphere is ~12.4%, which is comparable to the results obtained for NC HA/carbon nanotubes (CNT) [26]. The results of the thermal and chemical analyses agree satisfactorily and confirm the validity of the general formula $Ca_{10}(PO_4)_6(OH)_2 \cdot xGO \cdot yH_2O$, where $x = 0.5$, 1.0, and 2.0 and $y = 7.4$–7.7 (Table 2), which was proposed for the synthesized HA/GO CM.

Scanning electron microscopy analysis of the composition and morphology of the synthesis products. The synthesized HA/GO CM had uniform composition and contained, along with the main components of CM (Ca, P, O, C), insignificant amounts of Si (~0.02 wt %) and Cl (~0.03 wt %) (Fig. 9). The presence of the Cl impurity was likely to be due to insufficient washing of the synthesis products.

The synthesis products after drying in air were a solid mass, which, in strength characteristics, resembled sintered ceramics. After milling of dried samples in a ball mill, the produced powder comprised particles 100–900 μm in size, which often had a flattened shape (Figs. 9a–9c). On the surface of such particle, there is roughness, which is probably caused by the fact that GO sheets incorporated in the bulk of HA are exposed to the surface (Fig. 9d). At higher magnification, the wavy surface of particles with individual larger bulges is observed (Fig. 9e).

The base of the synthesized CM containing only an insignificant amount of GO is HA forming agglomerates (~200 nm in size) of spindle-shaped intergrowths of NC HA (Fig. 10a). The CM structure forming by intergrowth of such agglomerates was nanoporous (Fig. 10a).

On the surface of HA/GO CM particles after milling, there are flat regions (Fig. 10b, arrows), which are likely to be due to GO sheet cracking, leading to the flattened shape of the CM particles after milling. The exposure of GO sheets to the surface of the HA/GO CM particles in the scanning electron microscopy images is performed either by significant parts of GO sheets (Fig. 10c (1)), or by edges of GO sheets (Fig. 10c (2)), with the larger part of sheets remaining in the bulk of HA/GO CM. The scanning electron microscopy images showed that the GO distribution in HA/GO CM is quite uniform and is not characterized by any ordering. In certain regions of HA/GO CM, there are accumulations of GO sheets in the bulk of CM (Fig. 10c (2)). The scanning electron microscopy images reasonably suggest the absence of mutual contacts of GO sheets throughout the bulk of HA/GO CM samples of the synthesized compositions with an insignificant (to 2 wt %) GO content.

RESULTS AND DISCUSSIONS

The results of the physicochemical analysis of the initial GO and the synthesis products in the systems $CaCl_2$–$(NH_4)_2HPO_4$–NH_3–H_2O (25°C) and $CaCl_2$–$(NH_4)_2HPO_4$–NH_3–H_2O–GO (25°C) suggest the following conclusions on the composition–synthesis conditions–structure–dispersity–properties relationships for the synthesized HA/GO CM and on the interaction between HA and GO in the course of the synthesis.

(1) According to the analysis data, the nanocarbon material GO used in the experiments was GO with insignificant exfoliation of carbon sheets. This GO contained amorphous carbon impurities and insignificant (within 0.05 wt %) amounts of Al, Ti, Si, S, and Fe impurities (Fig. 1). The insignificant exfoliation of GO carbon sheets was indicated by weak X-ray diffraction lines within the range $2\theta \sim 11°$. The rugose GO

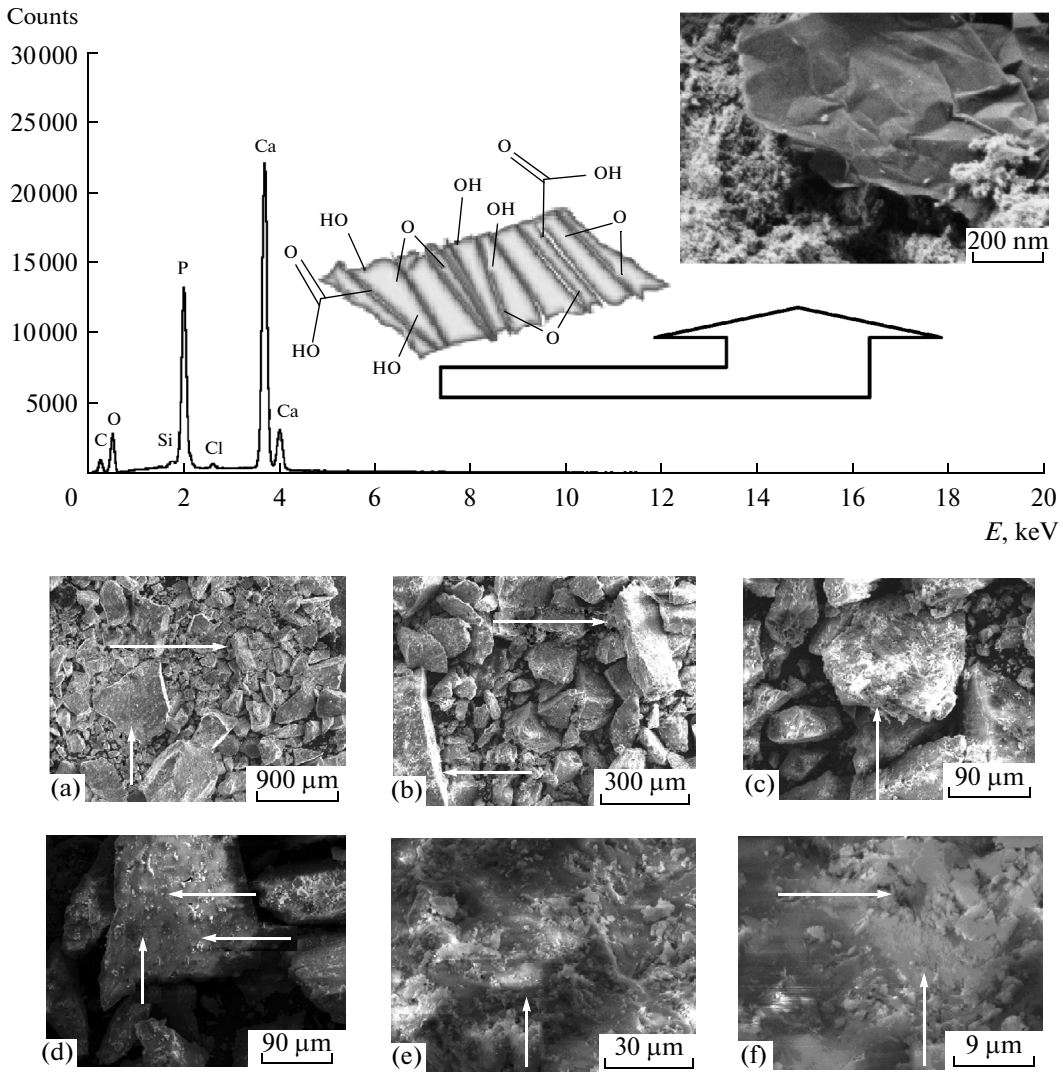

Fig. 9. Electron spectroscopy for chemical analysis showed that uniform samples of HA/GO CM of the composition $Ca_{10}(PO_4)_6(OH)_2 \cdot GO \cdot 7.4H_2O$ contain, along with the main components (Ca, P, O, C), also Si (~0.02 wt %) and Cl (~0.03 wt %). CM particles after milling have (a–c) a flattened shape and (d) a rough surface because of GO sheets incorporated in CM, which, at higher magnification, are seen to make the particle surface wavy (e).

sheets were detected by scanning electron microscopy (Fig. 1). The presence of amorphous carbon as agglomerates of particles ~200 nm in size was determined by transmission electron microscopy (Fig. 3). The IR spectra of the initial GO paste (Fig. 5, Table 1) used for the synthesis indicate that the GO contains adsorbed water and functional groups OH and COOH, which are active in interactions with ions in solution; these results agree satisfactorily with the data (Fig. 4) of the thermal analysis of the initial GO within the ranges of loss of water and OH^- and carbonate ions.

(2) In the test experiment, the synthesis in the system $CaCl_2$–$(NH_4)_2HPO_4$–NH_3–H_2O (25°C) in air gave NC HA of the stoichiometric (Ca : P = 1.67) composition (Table 2), containing carbonate ions CO_3^{2-}, which are substituted both for OH^- ions, and PO_4^{3-} groups of HA. The sizes (~23 × 12 nm along and across the hexagonal *c* axis, respectively) and composition of the synthesized nanocrystals of individual HA are close to those of bioapatite of the mammalian bone and dental tissues [11]. The chosen synthesis conditions enable one to obtain NC HA of smaller sizes than those (39 × 22 nm) in the synthesis in the system $Ca(OH)_2$–H_3PO_4–H_2O [26], with the habit of NC HA remaining almost unchanged at a length-to-width ratio of ~1.8.

(3) The coprecipitation of calcium and phosphorus salts in the system $CaCl_2$–$(NH_4)_2HPO_4$–NH_3–H_2O–GO (25°C), containing insignificant amounts of GO, produced nanosized hybrid HA/GO CM with the general formula $Ca_{10}(PO_4)_6(OH)_2 \cdot xGO \cdot yH_2O$,

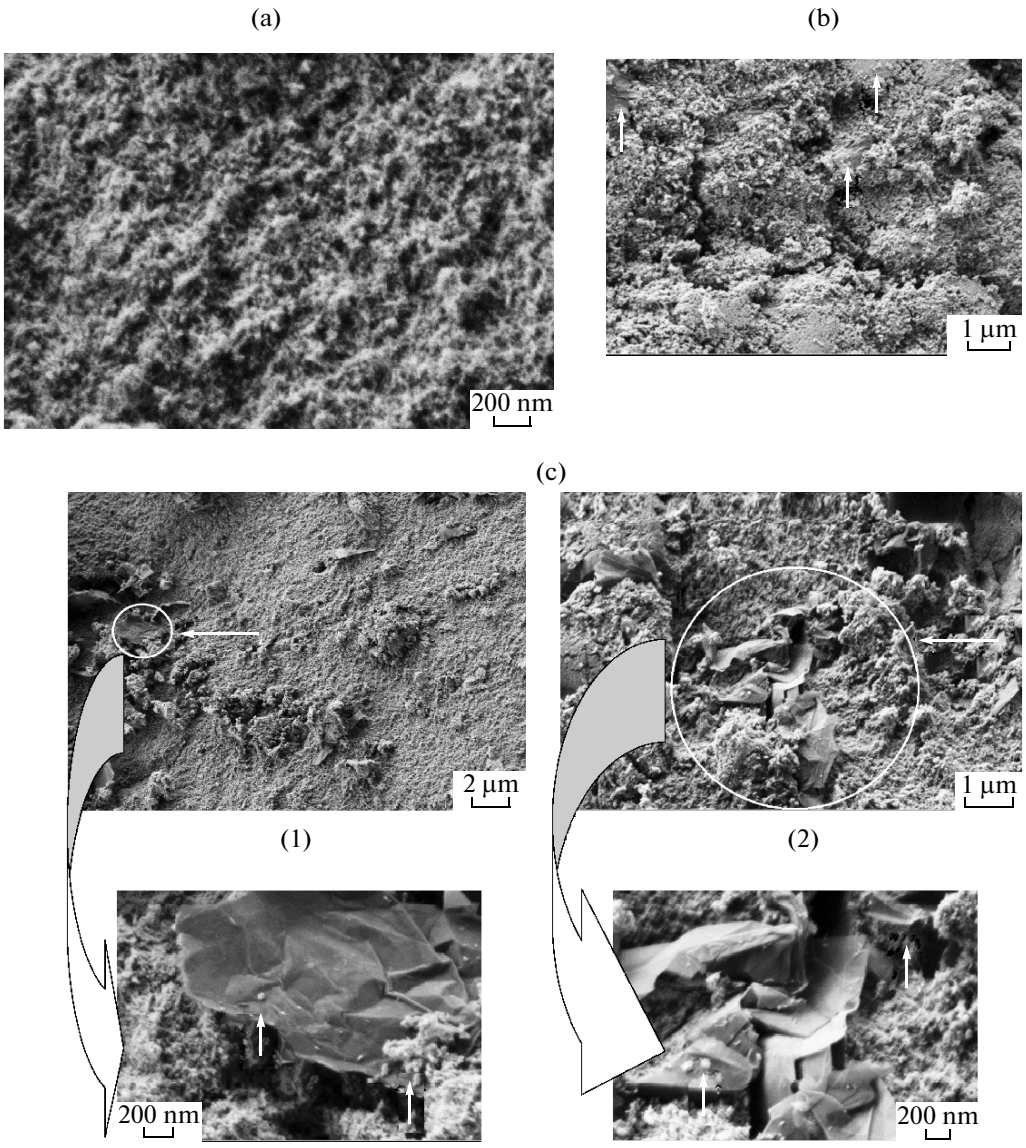

Fig. 10. (a) $Ca_{10}(PO_4)_6(OH)_2 \cdot GO \cdot 7.4H_2O$ include spindle-shaped intergrowths of NC HA. Flat regions (b, arrows) are likely to be due to GO sheet cracking. The exposure of GO sheets to the surface of the HA/GO CM particles is performed either (c (1)) by significant parts of GO sheets, or by (c (2)) edges of GO sheets, with the larger part of sheets remaining in the bulk of HA/GO CM.

where $x = 0.5$, 1.0, and 2.0 and $y = 7.4–7.7$ (Table 2). The chemical analysis of the synthesis products showed that all of the GO has interacted with calcium and phosphorus salts, the liquid after settling contains no residual GO (Table 2), and the activity of functional groups on the GO surface remains sufficient for GO to be completely bound by the forming NC HA.

(4) The presence of GO in the course of the NC HA crystallization hardly influenced the HA unit cell parameters (Table 4). The unit cell parameters of NC HA in HA/GO CM are close to the parameters of individual HA and do not differ from tabular data [23]. NC HA in HA/GO CM, as in the case of individual HA, contained carbonate ions CO_3^{2-}, substituted both for OH^- and PO_4^{3-} groups.

(5) At the same time, an increase in the GO content of HA/GO CM of the composition $Ca_{10}(PO_4)_6(OH)_2 \cdot xGO \cdot yH_2O$, where $x = 0.5$, 1.0, and 2.0 and $y = 7.4–7.7$, affects the sizes and morphology of NC HA (Fig. 11). The presence of even insignificant ($x = 0.5$) amounts of GO in CM leads to a decrease in the geometric sizes of NC HA both along and across the hexagonal c axis by ~30%, with the NC HA length-to-width ratio remaining ~1.85 in both cases (Table 4, Fig. 9). A further increase in the GO content of HA/GO CM to $x = 1.0$ hardly influences the HC HA

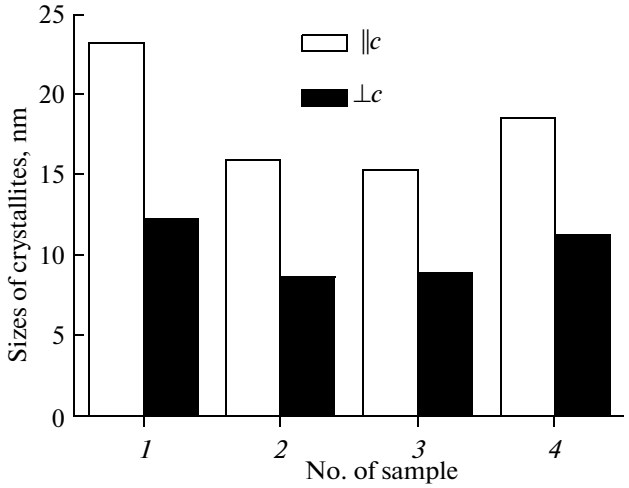

Fig. 11. Geometric characteristics of NC HA of (*1*) stoichiometric HA and HA in HA/GO CM of the composition $Ca_{10}(PO_4)_6(OH)_2 \cdot xGO \cdot yH_2O$, where x = (*2*) 0.5, (*3*) 1.0, and (*4*) 2.0 and $y = 7.4–7.7$. $\|c$ and $\perp c$ are the sizes of hexagonal NC HA along and across the hexagonal c axis, respectively.

sizes. However, an increase in the GO content of HA/GO CM to $x = 2.0$ leads to an increase in the longitudinal and transverse sizes of NC HA, with the longitudinal sizes increasing more significantly (~30%) than the transverse ones (~17%) (Fig. 9).

The initial decrease in the sizes of NC HA in HA/GO CM in comparison with individual HA is similar to the decrease in the sizes of NC HA in HA/CNT CM [26]. This decrease is probably determined by the emergence of additional crystallization nuclei under the conditions of batch crystallization in solution [27]. The difference of the effect of GO on the HA crystallization from solution from the effect of CNT is a certain increase in the sizes of NC HA in HA/GO CM with increasing GO content and in a tendency toward an increase in the sizes of hexagonal prisms of NC HA across the crystallographic c axis (the length-to-width ratio of NC HA in CM of the composition $Ca_{10}(PO_4)_6(OH)_2 \cdot xGO \cdot yH_2O$, where $x = 0.5$, is ~1.6). This may be related to the effect of active functional groups (OH, COOH) on the surface and,

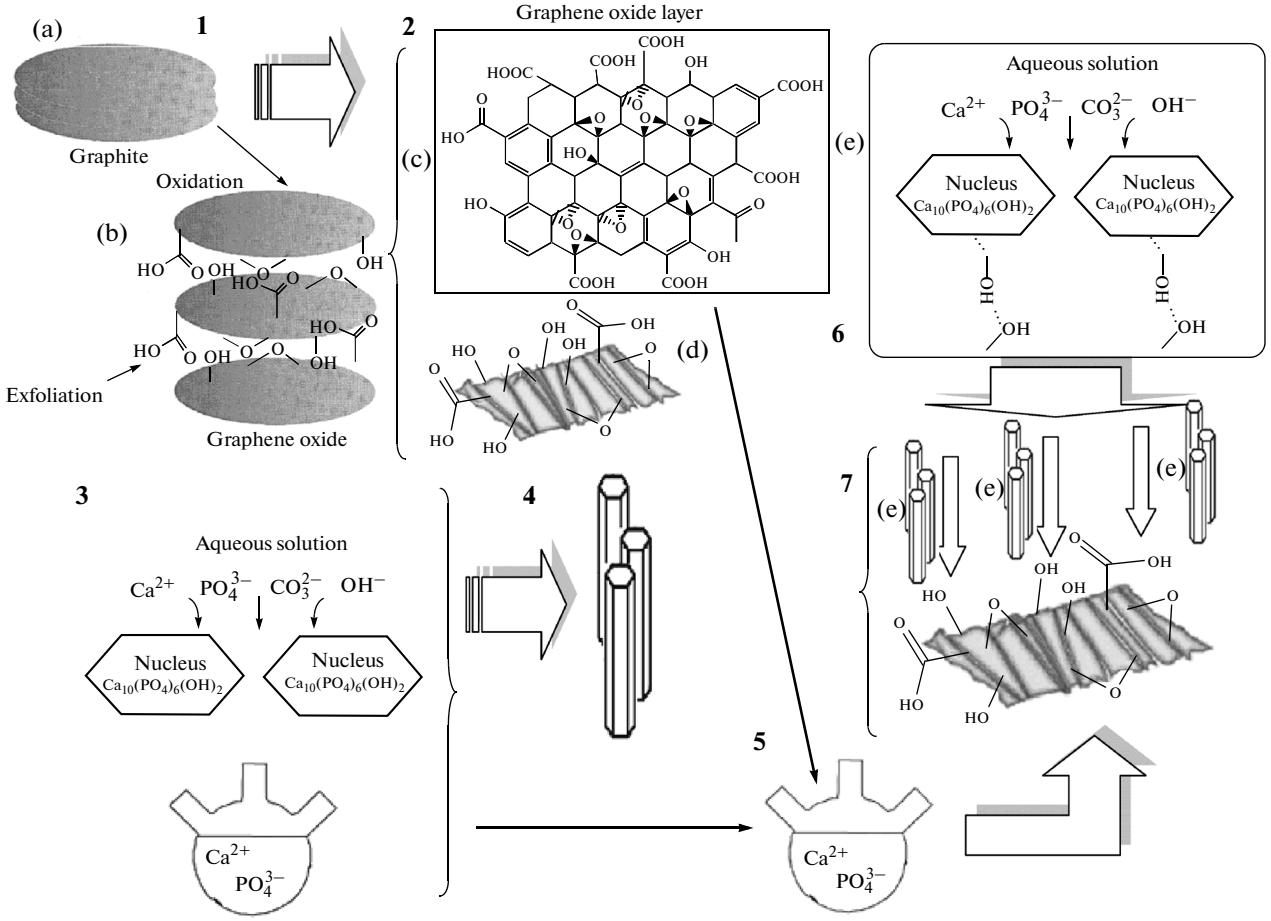

Fig. 12. (1, a) Graphite is transformed to (1, b) graphene oxide with (2, c) functionalized (2, d) rugose layers. The interaction between (2) GO and (3) calcium and phosphorus salts in the course of the synthesis to form (4) hydroxyapatite and (5) HA/GO CM in the coprecipitation of (6, e) HA and (7) GO.

first of all, on the edges of GO sheets (Fig. 10) participating in the formation of HC HA faces.

(6) Unlike HA/CNT CM [26], HA/GO CM are less heat-resistant. Heating them to 400°C is accompanied by a weight loss of ~8 wt %. At the same time, heating (1000°C, 1 h) of both individual NC HA and HA in either HA/GO CM or HA/CNT CM is accompanied by a similar process of agglomeration to form crystallites of intergrown NC HA ~200 nm in size.

(7) The presence of accompanying impurities and not too high quality of nanocarbon material could not, in our opinion, significantly influence the behavior of the model of the interaction between HA and GO; conversely, this created the real picture of the effect of GO and its synthesis by-products on the formation of NC HA in the presence of significant amounts of GO. Obtained in the in vitro experiments, the results of HA biomineralization in the presence of GO suggest the possible influence of GO on the sizes and morphology of NC HA of the native bone tissue in the case of deliberate or accidental participation of GO in metabolic processes.

Thus, the system $CaCl_2$–$(NH_4)_2HPO_4$–NH_3–H_2O–GO (25°C) was studied by the solubility method (Tananaev's residual concentration method) and by pH measurements and was used to model in vitro the biomineralization of the main inorganic component of the bone tissue—calcium hydroxyapatite $Ca_{10}(PO_4)_6(OH)_2$—in the presence of a nanosized modification of carbon—graphene oxide (Fig. 12). The conditions were determined for producing composite materials based in HA and GO with the general formula $Ca_{10}(PO_4)_6(OH)_2 \cdot x$GO $\cdot y H_2O$, where $x = 0.5$, 1.0, and 2.0 and $y = 7.4$–7.7. By chemical analysis, X-ray powder diffraction analysis, IR spectroscopy, thermogravimetric analysis, and differential scanning calorimetry, it was shown that nanosized crystals of HA in the synthesized HA/GO CM have a hexagonal symmetry and contain carbonate ions–, which are partially substituted both for OH^- and PO_4^{3-} ions (types A and B substitutions, respectively). The presence of GO in the course of the HA crystallization from solutions hardly affected the NC HA unit cell parameters. At the same time, with increasing GO content of HA/GO CM, there is a certain tendency toward an increase in the sizes of NC HA, both longitudinal and transverse. Obtained in the in vitro experiments, the results of HA biomineralization in the presence of GO suggest the possible effect of GO on the sizes and morphology of NC HA of the native bone tissue in the case of deliberate or accidental participation of GO in metabolic processes.

ACKNOWLEDGMENTS

This work was supported in part by the Presidium of the Russian Academy of Sciences (program "Fundamental Sciences for Medicine") and the Division of Chemistry and Materials Science of the Russian Academy of Sciences.

REFERENCES

1. V. C. Sanchez, A. Jachak, R. H. Hurt, et al., Chem. Res. Toxicol. **25**, 15 (2012).
2. A. Sasidharan, L. S. Panchakarla, P. Chandran, et al., Nanoscale **3**, 2461 (2011).
3. O. Akhavan and E. Ghaderi, ACS Nano **4**, 5731 (2010).
4. Y. Zhang, S. F. Ali, E. Dervishi, et al., ACS Nano **4**, 3181 (2010).
5. K.-H. Liao, Y.-S. Lin, C. W. Macosko, et al., ACS Appl. Mater. Interfaces **3**, 2607 (2011).
6. Y. Li, Y. Liu, Y. Fu, et al., Biomater. **33**, 402 (2012).
7. Y. Chang, S.-T. Yang, J-H. Liu, et al., Toxicol. Lett. **200**, 201 (2011).
8. H. P. Boehm, A. Clauss, G. O. Fischer, et al., Z. Naturforsch. B. **17**, 150 (1962).
9. G. Eda and M. Chhowallal, Adv. Mater. **22**, 2392 (2010).
10. http://patentscope.wipo.int/search/en/result.jsf] (front page search on "grapheme").
11. L. L. Hench, J. Am. Ceram. Soc. **81**, 1705 (1998).
12. M. Wei, J. H. Evans, and T. Bostrom, J. Mater. Sci.: Mater. in Medicine **14**, 311 (2003).
13. N. A. Zakharov, T. V. Belyaevskaya, and A. E. Chalykh, Kondens. Sredy Mezhfaz. Granitsy **8**, 18 (2006).
14. V. P. Orlovskii, G. E. Sukhanova, and Zh. A. Ezhova, Zh. Ros. Khim. o–va im. D.I. Mendeleeva **36** (6), 683 (1991).
15. S. V. Dorozhkin, Biomatter **1**, 121 (2011).
16. L. Stryer, *Biochemistry* (Freeman, New York, 1981).
17. W. S. Hummers and R. E. Offeman, J. Am. Chem. Soc. **80**, 1339 (1958).
18. N. I. Kovtyukhova, P. J. Ollivier, B. R. Martin, et al., Chem. Mater. **11**, 771 (1999).
19. P. Mahanandia, P. Vishwakarma, K. Nanda, et al., Mater. Res. Bull. **41**, 2311 (2006).
20. V. Labunov, B. Shulitski, A. Prudnikava, and K. Yanushkevich, J. Phys.: Conf. Ser. **100** 052095 (2008), http://dx.doi.org/10.1088/1742-6596/100/5/052095.
21. W. Li, C. Liang, W. Zhou, et al., J. Phys. Chem. B **107**, 6292.
22. V. P. Orlovskii, Zh. A. Ezhova, G. V. Rodicheva, et al., Zh. Neorg. Khim. **37**, 881 (1992).
23. ICPDS. 1980. File no. 9-432.
24. N. A. Zakharov, A. E. Chalykh, V. T. Kalinnikov, et al., Kondens. Sredy Mezhfaz. Granitsy **9**, 112 (2007).
25. Zh. A. Ezhova, N. A. Zakharov, E. M. Koval', and Kalinnikov V.T, Russ. J. Inorg. Chem. **54**, 477 (2009).
26. N. A. Zakharov, M. Yu. Sentsov, A. E. Chalykh, et al., Prot. Met. Phys. Chem. Surf. **49**, 80 (2013).
27. T. A. Larichev, T. V. Sitnikov, B. A. Sechkarev, et al., *Batch Crystallization in Inorganic Systems* (Kuzbassvuzizdat, Kemerovo, 2006) [in Russian].

Translated by V. Glyanchenko